Journal of Materials Chemistry A

ROYAL SOCIETY OF CHEMISTRY

COMMUNICATION

View Article Online
View Journal | View Issue

Cite this: J. Mater. Chem. A, 2024, 12, 6875

Received 29th October 2023
Accepted 9th January 2024

DOI: 10.1039/d3ta06602a

rsc.li/materials-a

Adsorptive molecular sieving of aromatic hydrocarbons over cyclic aliphatic hydrocarbons *via* an intrinsic/extrinsic approach†

Gengwu Zhang,‡[a] Xuanfu Zhu,‡[a] Lukman O. Alimi,[a] Xin Liu,[a] Aiping Chen,[b] Basem M. Moosa [a] and Niveen M. Khashab *[a]

Trianglimine (**TI**) and trianglamine (**TA**) macrocycles offer an efficient adsorptive molecular sieving strategy to separate toluene (**Tol**) from an equimolar mixture of **Tol** and methylcyclohexane (**MCH**) with 98.3% and 96.4% selectivity, respectively. Selective separation is achieved through the intrinsic cavity or extrinsic channel within the crystalline molecular absorbents, driven by C–H···π and π···π interactions. Moreover, **TI** and **TA** exhibit exceptional recyclability, highlighting their potential for sustainable chemical separation processes.

Cyclic aliphatics, such as cycloalkanes and alkyl-cycloalkanes, are often used as high-performance jet fuels and endothermic fuels to overcome the severe "thermal barrier" issue for hypersonic vehicles.[1,2] Among them, methylcyclohexane (**MCH**), a typical hexatomic ring alkyl-cycloalkane with the simplest branched structure, is frequently chosen as a jet-fuel surrogate for many practical fuels.[3–5] In chemical industry production, **MCH** is predominantly obtained through the hydrogenation of the corresponding aromatic toluene (**Tol**), resulting in the presence of unreacted **Tol**.[6] The separation of residual **Tol** from **MCH** is crucial for producing high grade **MCH**. However, conventional extraction and distillation methods face significant challenges in the separation of cyclic aliphatic and aromatic hydrocarbons due to their similar physical properties, such as close boiling points (384 K for **Tol** and 374 K for **MCH**) and the formation of azeotropes.[7] Consequently, developing sustainable and efficient technology for separating cyclic aliphatic and aromatic hydrocarbons becomes imperative in addressing these challenges.

Porous materials-based adsorptive separation technology has been recognized as an alternative strategy for the separation of cyclic aliphatic and aromatic hydrocarbons, owing to its high efficiency and low energy consumption.[8–23] In recent years, various adsorbents such as metal–organic frameworks (MOFs),[24] porous organic molecular frameworks (POMFs),[25] organic macrocycles,[26–28] and molecular cages[29] have been reported for the separation of **MCH** and **Tol**. Typically, these examples showed that **MCH** and **Tol** could be selectively adsorbed into the extrinsic void of assembled materials or the intrinsic cavity of macrocycles, depending on the differences in their molecular sizes, conformational structures, and electrical charge distributions. However, different separation mechanisms between the adsorption in the intrinsic cavity and extrinsic void are still unclear at the molecular level. Therefore, understanding the different host–guest complexation modes during separation is essential for developing novel adsorbents and exploring new separation strategies.

Herein, we present that the simple trianglimine (**TI**) and trianglamine (**TA**) macrocycles can be used for the separation of **MCH** and **Tol** by different adsorption behaviors (Fig. 1). **TI** exhibits a rigid molecular structure that enables the adsorption of the **Tol** molecule into its intrinsic cavity, while **TA**, with a flexible conformation, forms extrinsic channels in the crystalline assembly structure to capture the **Tol** molecule. Notably, to the best of our knowledge, this is the first example of conformational transitions being introduced to modulate adsorption occurring in the intrinsic cavity and extrinsic void.

TI and **TA** macrocycles were synthesized using the published methods,[30,31] respectively, and the purity of products was confirmed through ^{1}H NMR and ^{13}C NMR (Fig. S1–S4†). The crystalline **TI** and **TA** materials were obtained through recrystallization of their ethyl acetate solutions, followed by activation at 90 °C under vacuum for 12 hours to remove residual solvent molecules. Thermogravimetric analysis (TGA) and powder X-ray diffraction (PXRD) analysis indicated that both activated **TI** and **TA** displayed excellent thermal stability (Fig. S5 and S6†) and persistent crystallinity (Fig. S7 and S8†) after the activation.

[a]*Smart Hybrid Materials Laboratory (SHMs), Advanced Membranes and Porous Materials Center (AMPMC), King Abdullah University of Science and Technology (KAUST), Thuwal, 23955-6900, Saudi Arabia. E-mail: niveen.khashab@kaust.edu.sa*

[b]*Clean Combustion Research Center (CCRC), King Abdullah University of Science and Technology (KAUST), Thuwal 23955-6900, Saudi Arabia*

† Electronic supplementary information (ESI) available. CCDC 2287895 and 2287896. For ESI and crystallographic data in CIF or other electronic format see DOI: https://doi.org/10.1039/d3ta06602a

‡ These authors contributed equally to this work.

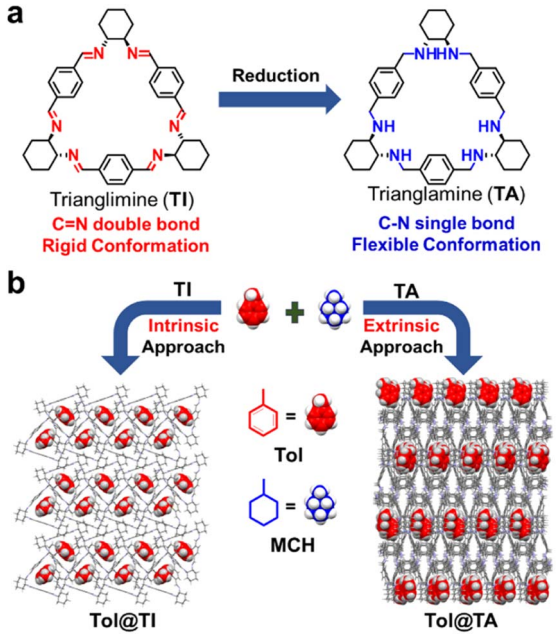

Fig. 1 (a) Chemical structures of TI and TA and their transformation. (b) Schematic illustration of the intrinsic and extrinsic capture approaches of Tol from the mixture of Tol/MCH by TI and TA.

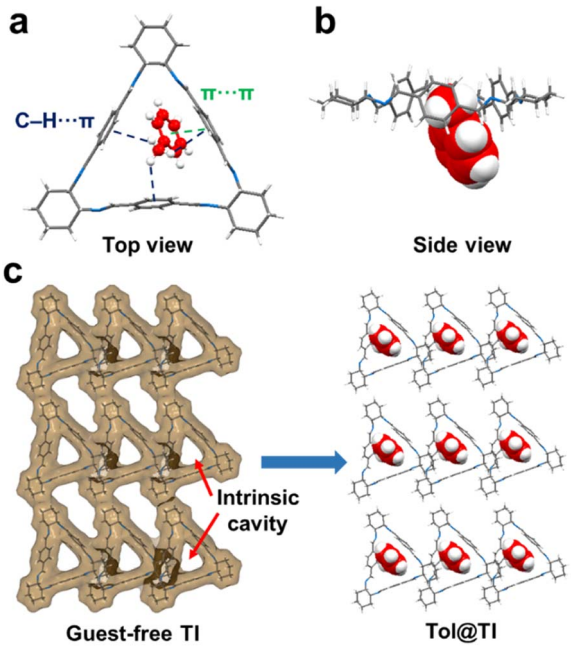

Fig. 2 (a) Top view and (b) side view of the single crystal structure of the asymmetric unit of Tol@TI. Blue dashed lines present the C–H···π noncovalent interactions existing between the guest molecule and TI. The green dashed line presents the π···π noncovalent interaction existing between the guest molecule and TI. (c) Single layer crystal packing structure along the crystallographic *a* axis with the contact surfaces of guest-free TI showing guest accessible voids within the intrinsic cavities and the complexation to Tol.

Furthermore, the N_2 sorption isotherm at 77 K demonstrated that the activated **TI** and **TA** crystals were not porous to N_2 at 77 K, exhibiting a Brunauer–Emmett–Teller (BET) surface area of 1.68 $m^2\ g^{-1}$ for **TI** (Fig. S9†) and 6.99 $m^2\ g^{-1}$ for **TA** (Fig. S10†), respectively.

To investigate the host–guest binding behaviors of guest molecules in **TI** and **TA**, efforts were made to grow single crystals of the macrocycles with **Tol** and **MCH**, followed by single crystal X-ray diffraction (SCXRD) analysis to gain a better understanding of the host–guest interactions. Specifically, by dissolving **TI** in a pure **Tol** solution and allowing it to cool/evaporate at room temperature for several days, colorless cubic crystals of **Tol@TI** were formed. The SCXRD analysis revealed that **Tol@TI** crystallizes in a monoclinic system with a $P2_1$ space group (Table S1†). Each asymmetric unit of **Tol@TI** consisted of one **TI** host macrocycle and one **Tol** guest molecule (Fig. 2a and b). The host **TI** molecule exhibited a regular triangular structure with an intrinsic cavity. The guest **Tol** molecule was found to be partially located within the cavity of the **TI** macrocycle, with the methyl group positioned appropriately inside the cavity. Notably, the methyl group of **Tol** formed multiple C–H···π interactions (3.025 Å, 3.128 Å and 3.245 Å, Fig. S11†) individually with the three benzene rings in the **TI** cavity, and the benzene ring of **Tol** exhibited a π···π stacking interaction (3.257 Å) with one benzene group in the **TI** macrocycle (Fig. S12†). Moreover, the packing arrangement of **Tol@TI** along the crystallographic *a* axis reveals an inclined 1D packing structure (Fig. S13 and S14†). Additionally, from the guest-free single layer 2D packing structure, it clearly shows the guest-accessible voids within the intrinsic cavity of **TI** and their capacity to adsorb guest **Tol** molecules (Fig. 2c).

A single crystal of **Tol@TA** was obtained by the same method. SCXRD analysis revealed that **Tol@TA** crystallizes in an orthorhombic system with a $P2_12_12_1$ space group (Table S1†), which consists of three **TA** macrocycles and three **Tol** guest molecules within the asymmetric unit (Fig. 3a and b). In contrast to **TI**, **TA** with a highly flexible conformation exhibited a distorted zigzag structure (Fig. S15†), which restricted the volume of guest-accessible voids within its intrinsic cavity and consequently limited its ability to capture guest molecules (Fig. S16†). However, in the crystal packing structure, six **TA** macrocycles assembled to form a 1D extrinsic channel along the *c* axis through host–host C–H···π interactions, accommodating all **Tol** guest molecules within these voids (Fig. 3c, S17 and S18†). Two of the **Tol** guest molecules ($\mathbf{Tol_I}$ and $\mathbf{Tol_{II}}$) were situated between two adjacent **TA** host macrocycles ($\mathbf{TA_1}$ and $\mathbf{TA_2}$) and stabilized by C–H···π interactions between the methyl group of **TA** and benzene of **Tol** (Fig. S19 and S20†). The third **Tol** guest molecule $\mathbf{Tol_{III}}$ was linked by one **TA** macrocycle, as well as connected with the **Tol** guest molecule $\mathbf{Tol_I}$ (Fig. S21†). These host–guest and guest–guest interactions also resulted in the formation of **Tol** channels along the crystallographic *c*-axis, which is consistent with the extrinsic channels formed by **TA** (Fig. S22†).

The distinct host–guest complexation modes of **TI** and **TA** with **Tol** can be attributed to the structural differences between the two macrocycles. Specifically, **TI** with C=N double bonds exhibits a rigid molecular skeleton that enables it to maintain

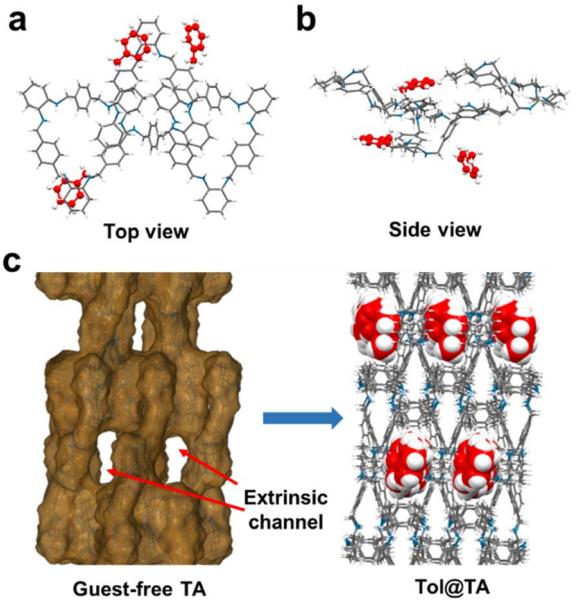

Fig. 3 (a) Top view and (b) side view of the single crystal structure of the asymmetric unit of Tol@TA. (c) Single layer crystal packing structure along the crystallographic *a* axis with the contact surfaces of guest-free TA showing the guest accessible voids within the extrinsic channels and the adsorption to Tol.

intrinsic cavities in the solid packing structure, thereby capturing guest molecules. However, upon reduction to **TA**, the rigid C=N double bonds are transformed into C–H single bonds, allowing for flexible rotation. As a result, **TA** adopts a more flexible conformation that makes it difficult to maintain guest accessible voids within its intrinsic cavities in the solid packing structure (Fig. S16†). Nevertheless, **TA** is more capable of forming extrinsic voids or channels to absorb guest molecules.

Subsequently, attempts were made to crystallize **TA** and **TI** with **MCH**. However, despite using various solvents and methods, all attempts were unsuccessful (Table S2†). This outcome may be attributed to **MCH**'s low electronegativity profile resulting from its non-aromatic structure, which limits its capacity to establish strong host–guest interactions with the host macrocycles (Fig. S39†). Specifically, **Tol** contains a CH_3 methyl group and an electron-rich benzene ring, which can not only form guest-to-host C–H···π interactions with the benzene rings on **TI** and **TA** but also can form additional π···π interactions and host-to-guest C–H···π interactions. In contrast, **MCH** solely comprises aliphatic hydrocarbon atoms, which can only form relatively weak guest-to-host C–H···π interactions with the benzene rings on **TI** or **TA**.

To further evaluate the potential of **TI** and **TA** as candidates for the adsorption of **Tol** and **MCH**, solid–vapor sorption experiments were performed on the activated **TI** and **TA** upon exposure to the single component of **Tol** and **MCH**, as well as their equimolar mixture, respectively. As revealed by ^{1}H NMR spectroscopy, each **TA** or **TI** macrocycle can capture approximately 0.9 molecules of **Tol** on average after reaching adsorption saturation (Fig. S23–S26†). In contrast, both **TI** and **TA** exhibited negligible uptake after being exposed to **MCH** vapors (Fig. S27 and S28†). The low adsorption capacity of **TI** and **TA** towards **MCH** explains the challenge in obtaining host–guest single crystals between **TA**/**TI** and **MCH**. Furthermore, PXRD experiments were conducted to investigate the structural changes of **TI** and **TA** after the uptake of **Tol** and **MCH**. The absorption of **Tol** molecules with activated **TI** and **TA** led to significant guest-induced structural changes, which were consistent with the simulated PXRD patterns of **Tol@TI** and **Tol@TA** (Fig. 3a and b). However, there were almost no changes in PXRD patterns for **TI** and **TA** after exposure to **MCH** vapor. Moreover, the different adsorption results were also verified through TGA analysis by comparing the relative weight loss of activated host macrocycles after absorbing **Tol** and **MCH** guest molecules, respectively (Fig. S29–S32†). These observations highlight the exceptional selectivity of **TI** and **TA** towards **Tol** over **MCH**.

Subsequently, equimolar mixtures of **Tol** and **MCH** were used to evaluate the separation performance of **TI** and **TA**. The results showed that the uptake of **Tol** in **TI** and **TA** increased over time and reached saturation within 20 h and 10 h, respectively (Fig. 4c, d, S33 and S34†). In contrast, **MCH** absorption was almost negligible throughout the entire experimental period for both **TI** and **TA**. Additionally, the PXRD patterns of **TI** and **TA** upon

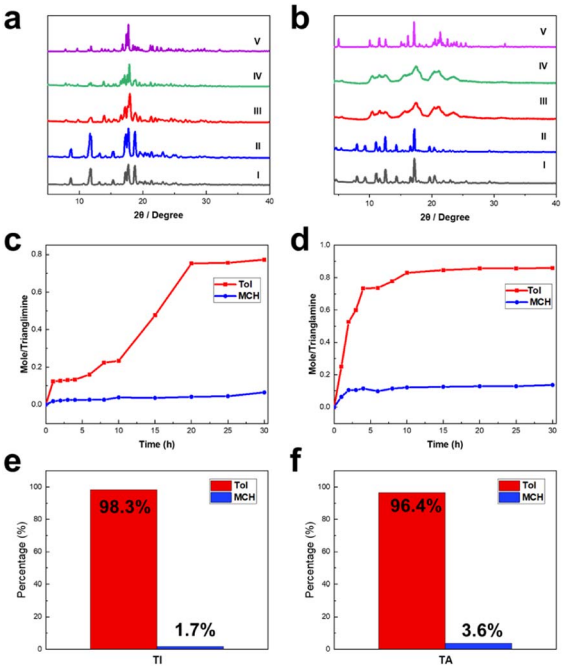

Fig. 4 (a) PXRD pattern of TI: (I) pure activated TI, (II) after absorption of MCH, (III) after absorption of Tol, (IV) after absorption of the Tol/MCH mixture, and (V) simulated from the single crystal structure of Tol@TI. (b) PXRD pattern of TA: (I) pure activated TA, (II) after absorption of MCH, (III) after absorption of Tol, (IV) after absorption of the Tol/MCH mixture, and (V) simulated from the single crystal structure of Tol@TA. (c) Time-dependent solid–vapor sorption curve of TI with a mix component of Tol/MCH. (d) Time-dependent solid–vapor sorption curve of TA with a mix component of Tol/MCH. (e) Relative uptakes of Tol/MCH in TI after saturated absorption. (f) Relative uptakes of Tol/MCH in TA after saturated absorption.

adsorption of **Tol**/**MCH** equimolar mixture vapor were in complete agreement with the patterns of **TI** and **TA** upon capturing **Tol** vapor and those simulated from **Tol@TI** and **Tol@TA** (Fig. 4a and b), respectively, implying the phase transformation from **TI** and **TA** into **Tol@TI** and **Tol@TA**. Furthermore, gas chromatography confirmed the high selectivity for **Tol** over **MCH**, with the proportion of **Tol** adsorbed in **TI** and **TA** reaching 98.3% and 96.4%, respectively (Fig. S35 and S36†).

In practical applications, the recyclability of absorbents is a crucial aspect that influences their potential use. For **TI** and **TA**, regeneration was achieved by heating the saturated samples at 90 °C under vacuum for 12 hours. Remarkably, the restored **TI** and **TA** samples maintained their selectivity towards **Tol** without any performance loss even after undergoing five cycles (Fig. S37†).

Conclusions

In conclusion, we have investigated the potential of **TI** and **TA** for the separation of aromatic **Tol** from aliphatic cyclic **MCH**. Both **TI** and **TA** exhibited high selectivity towards **Tol**, with adsorption capacities of 98.3% and 96.4%, respectively. Crystal structure analysis revealed that **TI**, with its rigid structure, could capture **Tol** through its intrinsic cavities, while the flexible conformation of the reduced product **TA** was able to assemble into extrinsic channels for absorbing guest molecules. This study demonstrates that altering the structure of a macrocycle can induce conformational changes to regulate intrinsic and extrinsic voids for separation. We expect that this research will not only provide a new strategy for designing novel absorbents but also inspire the application of supramolecular macrocycles in energy-intensive separation.

Conflicts of interest

There are no conflicts to declare.

Acknowledgements

We thank King Abdullah University of Science and Technology (KAUST) and the AMPM center for supporting this work.

References

1 Z. Wang, G. Liu and X. Zhang, *Fuel*, 2023, **331**, 125732.
2 B. W. Weber, W. J. Pitz, M. Mhel, E. J. Silke, A. C. Davis and C. J. Sung, *Combust. Flame*, 2014, **161**, 1972–1983.
3 B. Liu, Z. Wang, Q. Zhu, X. Li and J. Wang, *Fuel*, 2017, **200**, 387–394.
4 D. Hu, S. Zhang, C. Yang, G. Yao, Q. Zhu and Y. Chen, *J. Anal. Appl. Pyrolysis*, 2022, **168**, 105730.
5 F. Zhang, Z. Wang, Z. Wang, L. Zhang, Y. Li and F. Qi, *Energy Fuels*, 2013, **27**, 1679–1687.
6 L. Foppa and J. Dupont, *Chem. Soc. Rev.*, 2015, **44**, 1886–1897.
7 J. G. Villaluenga and A. T. Mohammadi, *J. Membr. Sci.*, 2000, **169**, 159–174.
8 M. Yamad, R. Yoshizaki, F. Uemura, H. Katagiri, S. Kato, K. Akimoto and F. Hamada, *Chem. Commun.*, 2023, **59**, 2604–2607.
9 P. F. Cui, X. R. Liu, Y. J. Liu, Z. H. Li and G.-X. Jin, *J. Am. Chem. Soc.*, 2022, **144**, 6558–6565.
10 J. Zhou, G. Yu, Q. Li, M. Wang and F. Huang, *J. Am. Chem. Soc.*, 2020, **142**, 2228–2232.
11 S. Mukjerjee, D. Sensharma, O. T. Qazvini, S. Dutta, L. K. Macreadie, S. K. Ghosh and R. Babarao, *Coord. Chem. Rev.*, 2021, **15**, 213852.
12 Y. Ding, L. O. Alimi, B. M. Moosa, C. Maaliki, J. Jacquemin, F. Huang and N. M. Khashab, *Chem. Sci.*, 2021, **12**, 5315–5318.
13 A. A. Sapianiki, K. A. Kovalenko, D. G. Samsonenko, M. O. Barsukova, D. N. Dybtsev and V. P. Fedin, *Chem. Commun.*, 2020, **56**, 8241–8244.
14 H. Yao, Y.-M. Wang, M. Quan, M. U. Farooq, L.-P. Yang and W. Jiang, *Angew. Chem., Int. Ed.*, 2020, **59**, 19945–19950.
15 C. G. Galán, A. L. Triguero, J. M. V. Luna, A. P. Zaderenko, A. Sławek, R. Sánchez-de-Armas and S. Calero, *Chem. Eng. J.*, 2020, **398**, 125678.
16 M. J. Emparan-Legaspi, J. Gonzalez, G. Gonzalez-Carrillo, S. G. Ceballos-Magañ, J. Canales-Vazquez, I. A. Aguayo-Villarreal and R. Muñiz-Valencia, *Microporous Mesoporous Mater.*, 2020, **294**, 109942.
17 L. K. Macreadie, O. T. Qazvini and R. Babarao, *ACS Appl. Mater. Interfaces*, 2021, **13**, 30885–30890.
18 H. L. Tan, Q. B. Chen, T. T. Chen and H. L. Liu, *ACS Appl. Mater. Interfaces*, 2018, **10**, 32717–32725.
19 Y. Han, Y. Chen, Y. Ma, J. Bailey, Z. Wang, D. Lee, A. M. Sheveleva, F. Tuna, E. J. L. Mclinnes, M. D. Frogley, S. J. Day, S. P. Thompson, B. F. Spencer, M. Nikiel, P. Manuel, D. Crawshaw, M. Schröder and S. Yang, *Chem*, 2023, **9**, 739–754.
20 A. Natraj, W. Ji, J. Xin, I. Castano, D. W. Burke, A. M. Evans, M. J. Strauss, M. Ateia, L. S. Hamachi, N. C. Gianneschi, Z. A. Alothman, J. Sun, K. Yusuf and W. R. Dichtel, *J. Am. Chem. Soc.*, 2022, **144**, 19813–19824.
21 M. Liang, S. Hu, N. Zhou, Z. Liu, Q. Chen, X. Chen, X. Liu, C. Li, J. Hao and P. Xue, *Small*, 2023, 2304340.
22 S. Mukjerjee, B. Manna, A. V. Desai, Y. Yin, R. Krishna, R. Babarao and S. K. Ghosh, *Chem. Commun.*, 2016, **52**, 8215–8218.
23 W. Yang, K. Samanta, X. Wang, T. U. Thikekar, Y. Chao, S. Li, K. Du, J. Xu, Y. Gao, H. Zuilhof and A. C.-H. Sue, *Angew. Chem., Int. Ed.*, 2020, **59**, 3994–3999.
24 L. K. Macreadie, R. Babarao, C. J. Setter, S. J. Lee, O. T. Qazvini, A. J. Seeber, J. Tsanaktsidis, S. G. Telfer, S. R. Batten and M. R. Hill, *Angew. Chem., Int. Ed.*, 2020, **59**, 6090–6098.
25 C. Chen, H. Guan, H. Li, Y. Zhou, Y. Huang, W. Wei, M. Hong and M. A. Wu, *Angew. Chem., Int. Ed.*, 2022, e202201646.
26 K. Jie, Y. Zhou, E. Li, R. Zhao and F. Huang, *Angew. Chem., Int. Ed.*, 2018, **57**, 12845–12849.
27 W. Wang, Z. Li, C. Song, J. Yang and Y. Yang, *Molecules*, 2022, **27**, 8554.

28 F. Zeng, X. S. Xiao, S. F. Gong, L. Yuan and L. L. Tang, *Org. Chem. Front.*, 2022, **9**, 4829–4833.
29 X. Zhao, Y. Liu, Z. Y. Zhang, Y. Wang, X. Jia and C. Li, *Angew. Chem., Int. Ed.*, 2021, **60**, 17904–17909.
30 M. Chadim, M. Budesinsky, J. Hodacova, J. Zavada and P. C. Junk, *Tetrahedron: Asymmetry*, 2001, **12**, 127–133.
31 J. Gawronski, K. Gawronska, J. Grajewski, M. Kwit, A. Plutecka and U. Rychlewska, *Chem.–Eur. J.*, 2006, **12**, 1807–1817.